# Nonlinear Hybrid Simulations of Energetic Particle Modes in Realistic Tokamak Flux Surface Geometry*)

Andreas BIERWAGE, Yasushi TODO[1)], Nobuyuki AIBA,
Kouji SHINOHARA, Masao ISHIKAWA and Masatoshi YAGI

*Japan Atomic Energy Agency, Naka 311-0193, Japan*
[1)]*National Institute for Fusion Science, Toki 509-5292, Japan*

(Received 22 December 2010 / Accepted 15 April 2011)

First results from nonlinear simulations of energetic particle modes and the resulting transport of energetic ions using realistic tokamak geometry are presented and compared with results obtained with a shifted-circle model equilibrium and otherwise equivalent parameters. The modes excited in both cases have similar frequencies and mode structures and cause a similar amount of energetic ion transport during the first few hundred Alfvén times of the nonlinear evolution. The similarity in transport is interesting since it stands in contrast to the reduced linear growth rate and saturation level in the non-circular case: for the parameters chosen, both are reduced by a factor of 2 compared to the circular case. These results motivate further studies, including a verification of our results with other codes, a clarification of the mechanisms underlying the linear stabilization, and a detailed analysis of the mode activity and particle redistribution during the nonlinear evolution.



Keywords: tokamak, equilibrium geometry, shear Alfvén wave, energetic particle mode, nonlinear simulation

DOI: 10.1585/pfr.6.2403109

## 1. Introduction

Nonlinear simulations are a useful and necessary tool to understand and interpret physical processes occurring when energetic ions interact with magnetohydrodynamic (MHD) modes in magnetically confined fusion experiments. Due to the approximations used, the quantitative predictive capabilities are still limited to relatively robust characteristics, such as the mode frequency range and mode structures. The predictions for the maximum amplitude and the amount of transport caused by the Alfvénic modes is expected to depend strongly on physical ingredients that have been ignored or strongly simplified, such as the magnetic flux surface geometry, free plasma boundary, and the interaction with kinetic bulk plasma dynamics.

While more advanced models and codes are under development, the state-of-the-art tools for global nonlinear simulations are still so-called hybrid codes, which treat the bulk plasma as an MHD fluid and follow the kinetic motion of energetic ion guiding centers. Due to their low density, the energetic ions enter mainly via the resonant and non-resonant contribution of their anisotropic pressure, while plasma inertia is mainly carried by the thermal bulk ions. Thus, the energetic ions may be taken to enter the MHD equations via the pressure-curvature coupling term only, requiring that the redistribution of energetic ions (and associated charge separation) be sufficiently small.

In this short paper, we present first results concerning the role of the magnetic flux surface geometry on the dynamics of energetic particle modes (EPM) [1, 2], with the purpose of indicating the direction for further work. We use the hybrid code MEGA [3, 4] in combination with the ideal MHD equilibrium code MEUDAS [5], which provides the equilibrium magnetic field geometry and bulk plasma pressure profile. The scenario considered is based on discharge E039672 in Japan Atomic Energy Research Institute Tokamak Upgrade, JT-60U, where the redistribution of energetic ions injected via negative neutral beams was studied during so-called Abrupt Large Events (ALE) and fast frequency sweeping (fast FS) modes [6]. We revisit previous simulations for this case, which were carried out by Briguglio *et al.* [7] in simplified geometry with circular magnetic flux surface cross-sections. This circular equilibrium model is also implemented in MEGA in order to carry out comparisons with the realistically shaped case. The modes of interest have low toroidal and poloidal mode numbers, $n = 1$ and $m = 1, ..., 4$, and frequencies in the range $30\,\mathrm{kHz} \lesssim f \lesssim 70\,\mathrm{kHz}$, which corresponds to $0.15 \lesssim \omega/\omega_{A0} \lesssim 0.35$ in on-axis Alfvén frequency units. The plasma profiles are shown in Fig. 1.

## 2. Model

MEGA solves the full MHD equations for the bulk plasma and a more detailed description may be found in Ref. [3]. In the present simulations, we choose to freeze the bulk density and pressure, $\rho$ and $P$, since their evolution cannot be adequately described by MHD for the frequency

*author's e-mail: bierwage.andreas@jaea.go.jp*

*) This article is based on the presentation at the 20th International Toki Conference (ITC20).

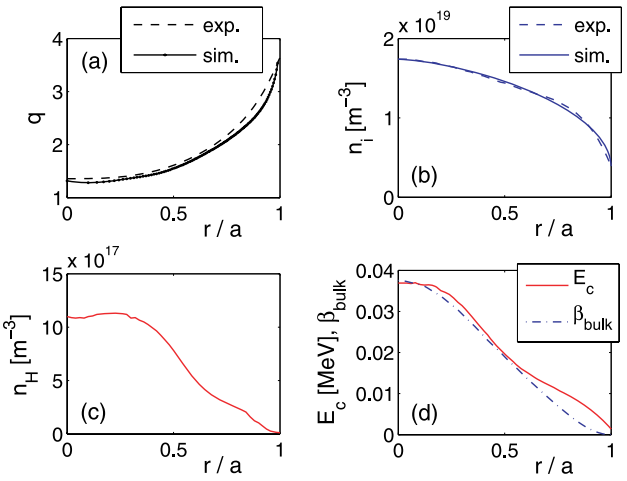


Fig. 1 Simulation setup: Radial profiles of (a) safety factor, (b) bulk ion density, (c) energetic ion density, (d) critical energy and bulk beta. $r/a$ is the volume-averaged radius.

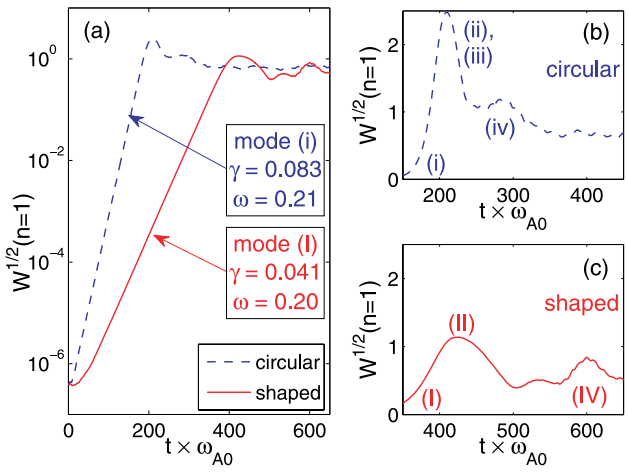


Fig. 2 Evolution of the $n = 1$ mode energy $W$: (a) log-scale plot and (b, c) linear-scale plots of the nonlinear evolution in the circular (dashed) and shaped case (solid). The labels (i)-(iv) in the circular case and (I)-(IV) in the shaped case refer to the dominant mode at a given time (cf. Fig. 3).

range at hand. The remaining equations describing the 3-dimensional dynamics of the bulk plasma are the equation for the $\boldsymbol{E}\times\boldsymbol{B}$ drift velocity $\boldsymbol{V}$ and magnetic field $\boldsymbol{B}$:

$$\rho\partial_t \boldsymbol{V} = -\rho\boldsymbol{\Omega}\times\boldsymbol{V} + \boldsymbol{J}\times\boldsymbol{B} - \nabla P - \nabla\cdot\hat{\boldsymbol{\Pi}}_{\rm H} - \frac{\rho}{2}\nabla V^2 - \nu\rho\nabla\times\boldsymbol{\Omega} + \frac{4}{3}\nu\rho\nabla(\nabla\cdot\boldsymbol{V}), \quad (1)$$

$$\partial_t \boldsymbol{B} = -\nabla\times\boldsymbol{E}; \quad (2)$$

where $\boldsymbol{E} = -\boldsymbol{V}\times\boldsymbol{B} + \eta\boldsymbol{J}$, $\mu_0\boldsymbol{J} = \nabla\times\boldsymbol{B}$, $\boldsymbol{\Omega} = \nabla\times\boldsymbol{V}$, and $\hat{\boldsymbol{\Pi}}_{\rm H}$ is the anisotropic pressure tensor computed from the perturbed energetic ion distribution function. A rigid, no-slip boundary condition ($\boldsymbol{V} = 0$) is imposed at the plasma surface. The energetic particles are modeled as guiding centers, with exactly conserved magnetic moment ($\partial_t\mu = 0$) and with the following equations governing the evolution of the guiding center location $\boldsymbol{R}_{\rm gc}$ and parallel velocity $v_\parallel$:

$$\partial_t \boldsymbol{R}_{\rm gc} = \boldsymbol{v}_\parallel^* + \boldsymbol{v}_{\rm E} + \boldsymbol{v}_B, \quad (3)$$

$$m_{\rm H} v_\parallel \partial_t v_\parallel = \boldsymbol{v}_\parallel^* \cdot [e_{\rm H}\boldsymbol{E} - \mu\nabla B]; \quad (4)$$

where $\boldsymbol{v}_\parallel^* = v_\parallel[\boldsymbol{B} + \rho_\parallel B\nabla\times\boldsymbol{b}]/B^*$, $\rho_\parallel = v_\parallel/\Omega_{\rm H}$ and $B^* = B(1+\rho_\parallel\boldsymbol{b}\cdot\nabla\times\boldsymbol{b})$. Particles crossing the plasma boundary are considered lost. The discretization of the fields is carried out on a cylindrical grid, $(R,\varphi,Z)$, the particles are represented by phase-space markers using the $\delta f$ weighting scheme, and the first-order particle-in-cell method is used for mapping between particle positions and grid nodes.

Beam ions in JT-60U are strongly anisotropic. However, for our first simulation, we choose to use only the isotropic component, $F_{\rm H}(r,v)$, of the local slowing-down distribution function previously employed in Ref. [7]:

$$F_{\rm H} = \frac{n_{\rm H}(r)}{\left[E_{\rm c}^{3/2}(r) + E_{\rm k}^{3/2}\right]\ln\left[1 + E_0^{3/2}/E_{\rm c}^{3/2}(r)\right]}; \quad (5)$$

where $E_{\rm k} = m_{\rm H}v^2/2$, $E_{\rm c}$ and $E_0$ are the kinetic, critical and birth energies, respectively. Since the profiles for the density and critical energy are functions of the volume-averaged minor radius $r$ and since markers are also initialized on loss orbits, $F_{\rm H}$ is not a true equilibrium and requires some time for "prompt relaxation", which occurs during the first approximately 100 Alfvén times. The central value of the energetic ion toroidal beta is $\beta_{\rm H0} = 0.035$ and the profile $\beta_{\rm H}(r)$ is similar to that of the critical energy, $E_{\rm c}(r)$, shown in Fig. 1 (d).

For comparability between the circular and shaped case, the relevant physical quantities must be equal or equivalent in both cases. In particular, the continuous shear Alfvén spectra, $\omega_{\rm A}(r)/\omega_{\rm A0}$, should differ only for frequencies above the toroidicity-induced gap (here, $\omega/\omega_{\rm A0} \gtrsim 0.4$). This is achieved by using the same profiles $q(r)$, $n_{\rm bulk}(r)$, $\beta_{\rm bulk}(r)$, and the same inverse aspect ratio, $a/R_0 = 0.29$; where $a$ is the minor radius in the circular case and the mean distance of the plasma boundary from the magnetic axis in the shaped case. In the shaped case, the outer 2% of the flux space are truncated to avoid the divertor X-point. In both cases, we use the same energetic ion distribution function $F_{\rm H}$ and the same ratio $v_0/(\omega_{\rm cH0}R_0) = 0.032$, where $v_0 = \sqrt{2E_0/m_{\rm H}}$ is a characteristic velocity and $\omega_{\rm cH0} = Z_{\rm H}eB_0/m_{\rm H}$ the cyclotron frequency of the energetic ions. The choice of an isotropic distribution, Eq. (5), implies that the comparison between circular and shaped equilibria is not sensitive to geometry-induced changes in the pitch angle of the dominant resonance, since all pitch angles have the same phase-space density.

## 3. Results

Results are presented in Figs. 2-6 for both circular and shaped cross-section. In Fig. 2, the evolution of the $n = 1$ mode amplitude (measured by the square root of kinetic mode energy, $W = m_{\rm i}n_{\rm i}\int {\rm d}^3x|\boldsymbol{V}|^2$) is shown. The labels (i)-

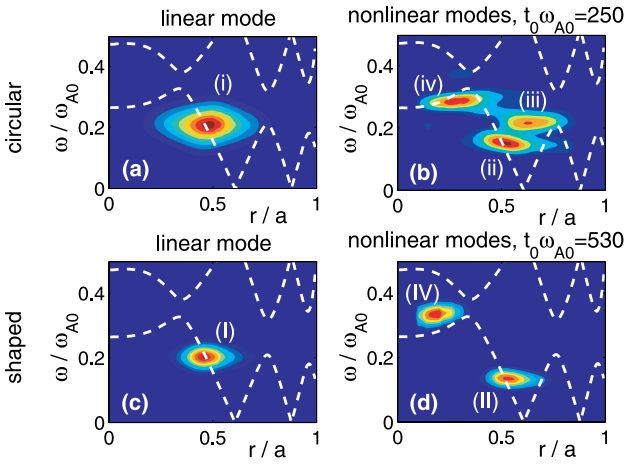


Fig. 3 Snapshot of the power spectrum contours of the electrostatic potential $\phi$ in (a, b) the circular and (c, d) the shaped case. (a) and (c) show the linear eigenmodes, (b) and (d) the nonlinear modes in the respective case. For the spectral analysis, a Hanning time window of width $200\omega_{A0}^{-1}$ around $t_0$ is used. The continuous spectrum (dashed) is computed from a large-aspect-ratio approximation.

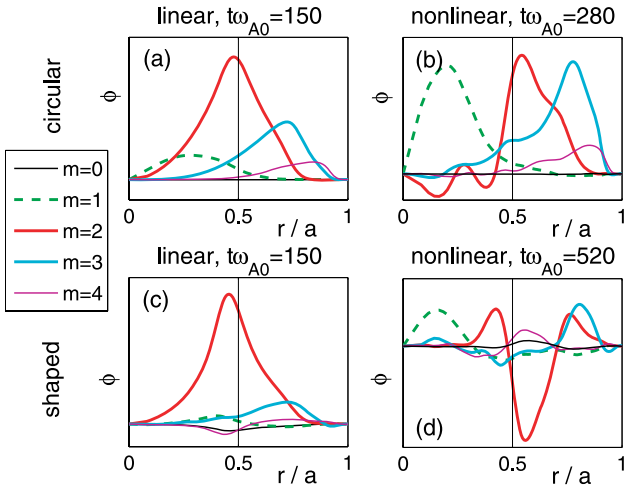


Fig. 4 Radial mode structure of individual poloidal harmonics $m = 0, 1, 2, 3, 4$ of the $n = 1$ component of the electrostatic potential $|\phi_{m,n}(r)|$ in (a, b) the circular and (c, d) the shaped case. (a) and (c) show the linear eigenmodes, (b) and (d) the nonlinear modes in the respective case.

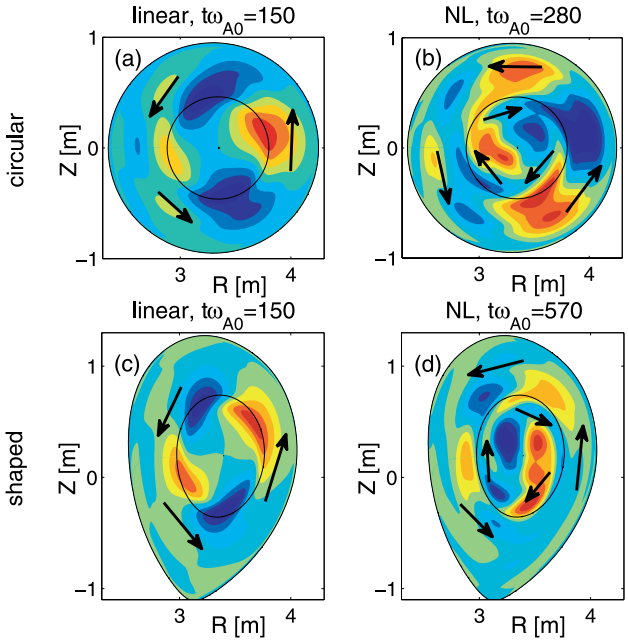


Fig. 5 Snapshot of the electrostatic potential $\phi_{n=1}(R, Z)$ mode structure contours in (a) the circular and (b) the shaped case. (a) and (c) show the linear eigenmodes, (b) and (d) the nonlinear modes in the respective case.

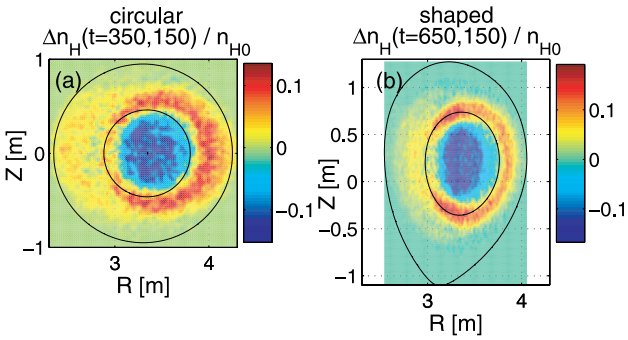


Fig. 6 Energetic ion density redistribution during the first two peaks of nonlinear $n = 1$ mode activity in (a) the circular and (b) the shaped case.

(iv) in the circular and (I)-(IV) in the shaped case indicate different modes, which dominate at different times. The power spectra in Fig. 3 show the frequency and radial location of the dominant modes during the linear (left) and nonlinear regime (right). The composition of the global mode structure from multiple poloidal harmonics $m = 0, ..., 4$ is shown in Fig. 4 and the structure in the poloidal plane is shown in Fig. 5. Changes in the energetic ion density are shown in Fig. 6.

In Fig. 2 (a) it is found that the linear growth rate in the shaped case is about 2 times lower than in the circular case. The saturation amplitude and the amplitude during the subsequent nonlinear evolution is also about 2 times lower than in the circular case. However, Fig. 2 (b, c) shows that the life-time of the peaks in the nonlinear regime of the shaped case is 2 times longer than in the circular case.

The linear mode is labeled (i, I). In both the circular case (Figs. 3-5, top) and the shaped case (bottom), the frequency of the linear modes is $\omega/\omega_{A0} = 0.2$ and the mode structures peak near $r/a \approx 0.5$. At this location, the frequency matches that of the $m = 2$ continuum and the energetic ion pressure has a steep gradient, so these modes are typical EPM. The smaller mode width in the shaped case may, at least partly, be explained by the lower linear growth rate competing with phase mixing (continuum damping).

The reason for the lower linear growth rate in the case

with non-circular flux surfaces remains to be determined. Such a stabilization may result from changes in continuum damping, field line connection length, drift orbit trajectories, or the coupling between field line curvature and energetic ion pressure tensor, through which the kinetic compression enters the MHD equations. Here, the field line connection length is similar in both cases and the linear mode frequency is a factor of 2-3 below the ellipticity-induced gap, so we expect continuum damping to be similar in both cases and focus our attention on the kinetic energetic ion compression and pressure-curvature coupling. Preliminary measurements of the energetic ion pressure field indicate that the ratio of pressure perturbations (normalized by mode amplitude) between shaped and circular cases lies in the range 0.6 to 0.9, indicating that the kinetic compression is indeed weaker in the shaped case. In addition, shaping-induced changes in the pressure-curvature coupling may affect EPMs in a similar way as MHD ballooning modes (e.g., see Fig. 5 in Ref. [8]). Further study with additional diagnostics are required to explain the different growth rates in the circular and shaped case.

During the nonlinear saturation phase, the EPM moves radially outward. In the circular case, we observe a superposition of two outward propagating components, which are captured by the snapshot shown in Fig. 3 (b). One component, labeled (ii), sweeps down in frequency, following the $m = 2$ continuum. The other component, labeled (iii), localizes near the lower accumulation point of the toroidicity-induced gap located at $r/a \approx 0.75$, which has a frequency similar to that of the linear EPM (i). Note that mode (iii) appears only transiently and it remains to be examined whether or not it couples to a toroidicity-induced Alfvén eigenmode (TAE) [9]. In the shaped case, shown in Fig. 3 (d), the down-sweeping component (II) dominates and its lowest frequency is about $\omega/\omega_{A0} = 0.11$.

While modes (ii, II) and (iii) decay, another mode, labeled (iv, IV) in Fig. 3 (b, d), appears in the region $0.1 \lesssim r/a \lesssim 0.4$ in both the circular and shaped case. Its frequency hovers around $0.3 \lesssim \omega/\omega_{A0} \lesssim 0.35$; that is, on or above the local $m = 1$ continuum and around the accumulation point of the toroidicity-induced gap near $r/a \approx 0.35$, where $m = 1$ and $m = 2$ couple. Viewed in the poloidal plane, the centralized mode (iv, IV) tends to rotate in the opposite direction compared to the other modes, as indicated by arrows in Fig. 5 (b, d).

The variable frequency and mode structure of mode (iv, IV) clearly indicates its EPM nature (as opposed to an MHD Alfvén eigenmode). Due to the weak magnetic shear near the magnetic axis, it can be expected that mode (iv, IV) is easily excited even with weak drive. Note, however, that the localization of mode (iv, IV) in a region where the energetic ion pressure gradient is small does not necessarily imply weak wave-particle interaction. The pressure contours of the resonant particles lie on surfaces of constant canonical toroidal momentum, $\boldsymbol{P} \cdot \boldsymbol{\nabla}\varphi = P_\varphi = e_H\psi + m_H v_\varphi$, which differ from flux contours, especially near the magnetic axis. Hence, mode (iv, IV) may play a significant role for energetic ion transport and should be analyzed in more detail.

A first impression of the spatial redistribution of energetic ions caused by all the modes described above is given in Fig. 6, where the change in the velocity-space-averaged energetic ion density field is shown. This result is obtained by subtracting the density field in the linear stage after prompt relaxation, $n_H(R, Z, t\omega_{A0}{=}150)$, from the density field found after the second peak in $n = 1$ mode activity ($t\omega_{A0} = 350$ in the circular and $t\omega_{A0} = 650$ in the shaped case). During that interval, the energetic ion density varies on the order ± 10% in both the circular and shaped case.

# 4. Conclusion

Summarizing the observations made, we find that the frequencies and structures of linear modes (i, I) and long-lived nonlinear modes (iv, IV) are similar in simplified circular geometry and realistically shaped geometry. The same counts for the frequency sweeping mode (ii, II). We expect that these robust results are most readily comparable to experimental data. In fact, as pointed out in Ref. [7], the range of frequencies obtained in the simulations, $0.11 \lesssim \omega/\omega_{A0} \lesssim 0.35$ ($22\,\text{kHz} \lesssim f \lesssim 70\,\text{kHz}$), is similar to the range of frequencies measured experimentally, indicating that the $q$ profile may have been estimated well. (Note that due to the low magnetic field strength in this discharge [6] the measurements of $q$ are not very accurate and $q(r = 0)$ may vary by $\pm 0.5$.)

Differences between the circular and shaped cases were found in the growth rate and the saturation amplitude of the linearly most unstable mode. In the examples studied, these are a factor of 2 lower in the shaped case than in the circular case. However, the life-time of the peaks of mode activity in the shaped case is a factor of 2 longer than in the circular case. This may be a reason for why, after the first two peaks of $n = 1$ mode activity, the redistribution of energetic ions is similar in both the circular and the shaped case.

The finding that transport is not reduced despite a reduced growth rate and saturation level is important for the interpretation of results based on linear and quasi-linear analyses, since it indicates that a stabilizing/destabilizing effect of certain geometric features (such as ellipticity and triangularity) does not imply less/more transport. A verification of this result with other codes is desirable, since conclusive convergence studies with respect to spatial resolution are computationally expensive with MEGA.

Building on the results presented in Ref. [7], the displacement of particles in radius and velocity space has to be examined in order to address the question whether the transport is of diffusive or ballistic kind. The relation between the nonlinear evolution of an EPM (frequency sweeping, radial spreading) and the evolution of the particle distribution function should be analyzed and compared

with theoretical predictions (for a review, see Ref. [10]).

## Acknowledgments

One of the authors (A.B.) would like to thank S. Briguglio for providing useful advice and benchmark data, and F. Zonca for useful discussions concerning the interpretation of the results. This work was partly supported by Grant-in-Aid for Scientific Research (Start-Up) from the Japanese Ministry of Education, Culture, Sports, Science and Technology, Grant No. 22860081.

[1] L. Chen *et al.*, Phys. Rev. Lett. **52**, 1122 (1984).
[2] L. Chen, Phys. Plasmas **1**, 1519 (1994).
[3] Y. Todo *et al.*, Phys. Plasmas **12**, 012503 (2005).
[4] Y. Todo, Phys. Plasmas **13**, 082503 (2006).
[5] M. Azumi *et al.*, Proc. 4th Intl. Symp. Comp. Methods Appl. Sci. Eng. Paris, 335 (1980).
[6] M. Ishikawa *et al.*, Nucl. Fusion **45**, 1474 (2005).
[7] S. Briguglio *et al.*, Phys. Plasmas **14**, 055904 (2007).
[8] R.L. Miller *et al.*, Phys. Plasmas **5**, 973 (1998).
[9] C.Z. Cheng, L. Chen and M.S. Chance, Ann. Physics **161**, 21 (1985).
[10] L. Chen and F. Zonca, Nucl. Fusion **47**, S727 (2007).